A comparative analysis of structural and luminescent properties of homoepitaxially and quasi-homoepitaxially grown LuAG:Ce single crystalline films under ambient and high pressure

A. Markovskyi[a]*, Yu. Syrotych[a], N. Majewska[b], M. Kamiński[b], V. Gorbenko[a], T. Zorenko[a], A. Wierzbicka[c], A. Suchocki[c], S. Mahlik[b], Yu. Zorenko[a*]

[a] Faculty of Physics, Kazimierz Wielki University in Bydgoszcz, Powstańców Wielkopolskich str., 2, 85090 Bydgoszcz, Poland

[b] Institute of Experimental Physics, Faculty of Mathematics, Physics and Informatics, University of Gdansk, Wita Stwosza 57, 80-308 Gdansk, Poland

[c] Institute of Physics, Polish Academy of Sciences, al. Lotnikow 32/46, 02-668 Warsaw, Poland

Abstract

This work is dedicated to investigating the structural, luminescence and photocurrent characteristics of LuAG:Ce single crystalline films (SCFs) grown using the Liquid Phase Epitaxy method on both LuAG and YAG substrates. The primary objective is to analyze the influence of different growth modes, namely *homoepitaxial (HE)* and *quasi-homoepitaxial (QHE)*, on the structural and luminescent properties of Ce^{3+} ions under ambient and high-pressure conditions. Based on the results of XRD measurements, we can conclude that both epitaxial structures *are fully relaxed*. However, a slight deformation of the garnet lattices is observed, manifesting the inequality of the *in-plane* and *out-of-plane* lattice constants of substrates and films. The difference in the energy gap values between positions of 4f-$5d_{1,2}$ Ce^{3+} absorption bands (6-12 meV) and the positions of Ce^{3+} emission band (6 meV) was observed for both LuAG:Ce films and caused by the small differences in local perturbations of garnet hosts for epitaxial structures, grown in HE and QHE modes. The Ce^{3+} emission intensity in LuAG:Ce HE and QHE films decreases with temperature in the 10-300 K range. The decay time of the Ce^{3+} luminescence in LuAG:Ce HE film demonstrates a weak temperature dependence in the mentioned range. However, in LuAG:Ce QHE grown film, the decay time of the Ce^{3+} emission shows notable temperature dependences in the 10-300 K range, probably due to the formation of Ce^{4+}-Pb^{2+} pair centers. The non-monotonical redshift of the Ce^{3+} emission band and the increse of the Ce^{3+} decay time are observed in both LuAG:Ce HE and QHE films under increasing external pressure from ambient to 19 GPa due to the compression and distortion of the crystal lattice. The redshift changes of the Ce^{3+} emission band on pressure are significantly more complicated for LuAG:Ce QHE-grown film than their HE counterpart. The outcomes of this study contribute to the fundamental understanding of epitaxial growth processes and their impact on the luminescence characteristics of rare-earth-doped materials in single crystalline film form.

KEYWORDS: Liquid phase epitaxy, single crystalline films, $Lu_3Al_5O_{12}$, X-ray diffraction, Ce^{3+} ions, luminescence, high-pressure

Introduction

In advanced optical devices, luminescent materials play a pivotal role in various applications, ranging from scintillation detectors for nuclear physics to high-performance phosphors in solid-state lighting [1, 2]. Lutetium Aluminum Garnet doped with Cerium $Lu_3Al_5O_{12}$:Ce (LuAG:Ce) stands as a remarkable representative of these luminescent materials, offering a unique blend of optical, scintillation, and mechanical properties that have spurred significant interest in recent years [3–5]. LuAG:Ce exhibits substantial differences in its luminescent and scintillating properties depending on its material form, whether it is bulk

crystalline, film, powder, or ceramic. These variations arise from each form's unique structural and microstructural characteristics, which significantly impact the performance and applications of LuAG:Ce [6–8]. Understanding of the differences in material forms is essential for tailoring LuAG:Ce to specific applications, optimizing its performance, and harnessing its full potential in the fields of scintillation detectors, radiation imaging, and optoelectronics.

Systematic studies of the structural and optical properties of single crystalline films (SCF) garnet compounds have been carried out since the 1980s and 1990s when the first Ce^{3+} doped $Y_3Al_5O_{12}$ (YAG:Ce) and LuAG:Ce SCFs were crystallized for different optoelectronic applications using the liquid phase epitaxy (LPE) growth method [9-14]. Namely, epitaxially grown SCFs of garnet compounds doped with Ce^{3+} ions show significant promise as a replacement for polished thin plates of single crystals in the context of 2D scintillation imaging screens with submicrometer spatial resolution and photoconverters for WLEDs [15–17]. They offer several advantages compared to single crystals (SCs) grown using the Czochralski (Cz) method. The liquid phase epitaxial (LPE) garnet films are grown from a flux near 1000°C, whereas the growth temperatures of Cz garnet crystals can reach as high as 2000°C. As a result, this lower growth temperature results in reduced structural disorder and fewer intrinsic crystal defects, such as antisite defects and oxygen vacancies, in the epitaxially grown films [18–20].

Conversely, the crystal lattice may experience the introduction of diverse impurities from the flux, and distinct defects specific to the LPE technology can emerge during the growth process. Additionally, factors such as flux properties (composition, viscosity), growth conditions (temperature, supercooling, growth rate), and substrate properties (lattice match between layers and substrates, presence of defects) can influence the quality of epitaxial layers and, consequently, impact their luminescent properties.

This study aims to delve into the structural and luminescence characteristics of LuAG:Ce SCFs grown using the LPE method onto LuAG and YAG substrates. The primary focus is to examine the impact of homoepitaxial (HE) and quasi-homoepitaxial (QHE) growth modes on the luminescent properties of Ce^{3+} ions in ambient and high pressure.

1. Sample preparation and experimental methods

The LuAG:Ce SCFs with thicknesses of 17 μm and 14 μm were grown using the LPE growth method from the melt-solutions based on the PbO-B_2O_3 flux onto LuAG and YAG substrates with (100) and (111) crystallographic orientations, respectively (Fig. 2). The substrates were prepared from the respective Cz-grown crystals using cutting, mechanical polishing, and final chemical mechanical polishing in SiO_2 slurry.

The starting PbO, B_2O_3, Lu_2O_3, CeO_2, and Al_2O_3 raw oxides of 4N purity were used for melt-solution preparation. The film growth was performed from the supercooled melt solution based on PbO-B_2O_3 (12:1 mole/mole) flux agents and garnet components, placed into a Pt crucible. The content of garnet components in the melt solutions was in the 2.5–3.0 mole % range. The solution's Lu_2O_3/Al_2O_3 oxide content was chosen with a stoichiometric ratio of 3/5. Due to very low segregation coefficients of Ce^{3+} ions in LuAG, the concentration of CeO_2 activating oxides in the melt-solution was equal to 10 mole % per total mole quantity of solution. The substrate rotation speed in the melt was 60–160 rpm. In all growth cycles, the growth temperature T_g was in the 950-975 ºC range, and the growth rate was in the f_s=0.2-0.5 μm/min range. The nominal Ce ion concentration in the film was about 0.15 at. %

X-ray diffraction (XRD) investigations were conducted utilizing a PANalytical X'Pert PRO MRD diffractometer featuring a hybrid two-bounce Ge (220) monochromator and a triple bounce Ge (220) analyzer positioned in front of the detector. Initially, θ-2θ XRD scans

encompassing a broad range of 2θ angles were performed to assess the crystallographic perfection of the SCF samples. Subsequently, high-resolution X-ray diffraction measurements were carried out to determine the lattice parameters and quality of LuAG:Ce SCFs. This involved the acquisition of ω and ω-2θ scans around both symmetrical and asymmetrical reflections, leading to the derivation of reciprocal space maps.

Optical absorption spectra of the investigated samples were recorded in the 200-1100 nm range using a Jasco 760 UV-Vis spectrometer. The room temperature (RT) photoluminescence (PL) and photoluminescence excitation (PLE) spectra were measured with a FluoroMax-4P (Horiba) equipped with a 150 W xenon lamp as the excitation source and an R928 Hamamatsu photomultiplier as the detector which allows to record spectrum in the range of 250–850 nm. High-pressure emission measurements were performed with an Andor SR-750-D1 spectrometer with a CCD camera DU420A-OE type. The excitation source was a He-Cd laser with a 442 nm wavelength. Elevated hydrostatic pressure was generated inside a Merrill Bassett-type diamond anvil cell (DAC) [21]. Polydimethylsiloxane oil was employed as the pressure-transmitting medium, and pressure quantification was achieved by observing the shift of the R1 luminescence line in ruby (Al_2O_3:Cr) [22]. The sample loaded to the DAC was a piece broken off from the entire epitaxial structure since the thickness of the sample in the cell cannot exceed 25 μm. The sample was selected under a microscope to make the film and the substrate visible.

Photocurrent excitation spectra (PCE) were conducted utilizing a specifically designed experimental arrangement. This setup comprised a 150 W xenon lamp (LOT quantum design) connected to a grating monochromator (Omni-λ 1509) covering the spectral range of 250-1000 nm as an excitation source. A digital electrometer (Keysight B2987A) was employed for photocurrent measurement. To enhance the signal-to-noise ratio, modulation of the excitation light at 5 Hz was achieved using an optical chopper, while the photocurrent signal was isolated via a lock-in amplifier (Signal Recovery 7270, Ametek Scientific Instruments).

2. Results and discussion

2.1. Structural properties of LuAG:Ce SCFs

Fig. 1 shows the crystal structure of pure LuAG. The LuAG host has a cubic crystal structure with space group *Ia3d* (230). Its conventional cell contains 160 atoms with Lu in 24 (c) eightfold coordinated sites, Al in 16 (a) sixfold coordinated and 24 (d) fourfold coordinated sites, and O in 96 (h) sites.

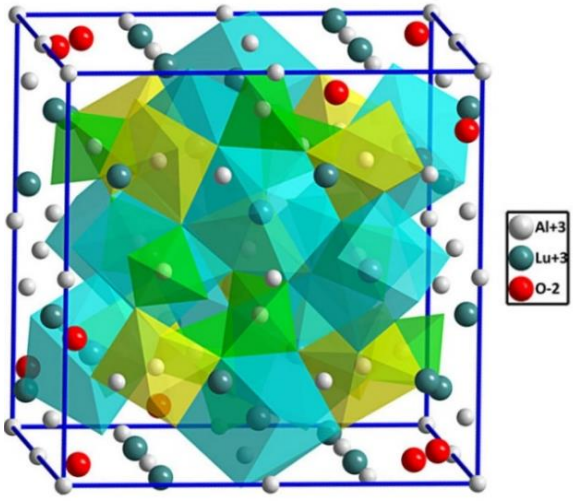

Fig.1. Crystal structure of $Lu_3Al_5O_{12}$ (space group: *Ia3d*, the Lu atoms occupy the 24 (c) sites, the O atoms occupy the 96 (h) sites, Al atoms occupy the 16 (a) sites and 24 (d) sites).

The X-ray diffraction pattern of the LuAG:Ce SCF/LuAG SC HE structure and LuAG:Ce SCF / YAG SC QHE structure are shown in Fig.2a, b and 2 c, d, respectively.

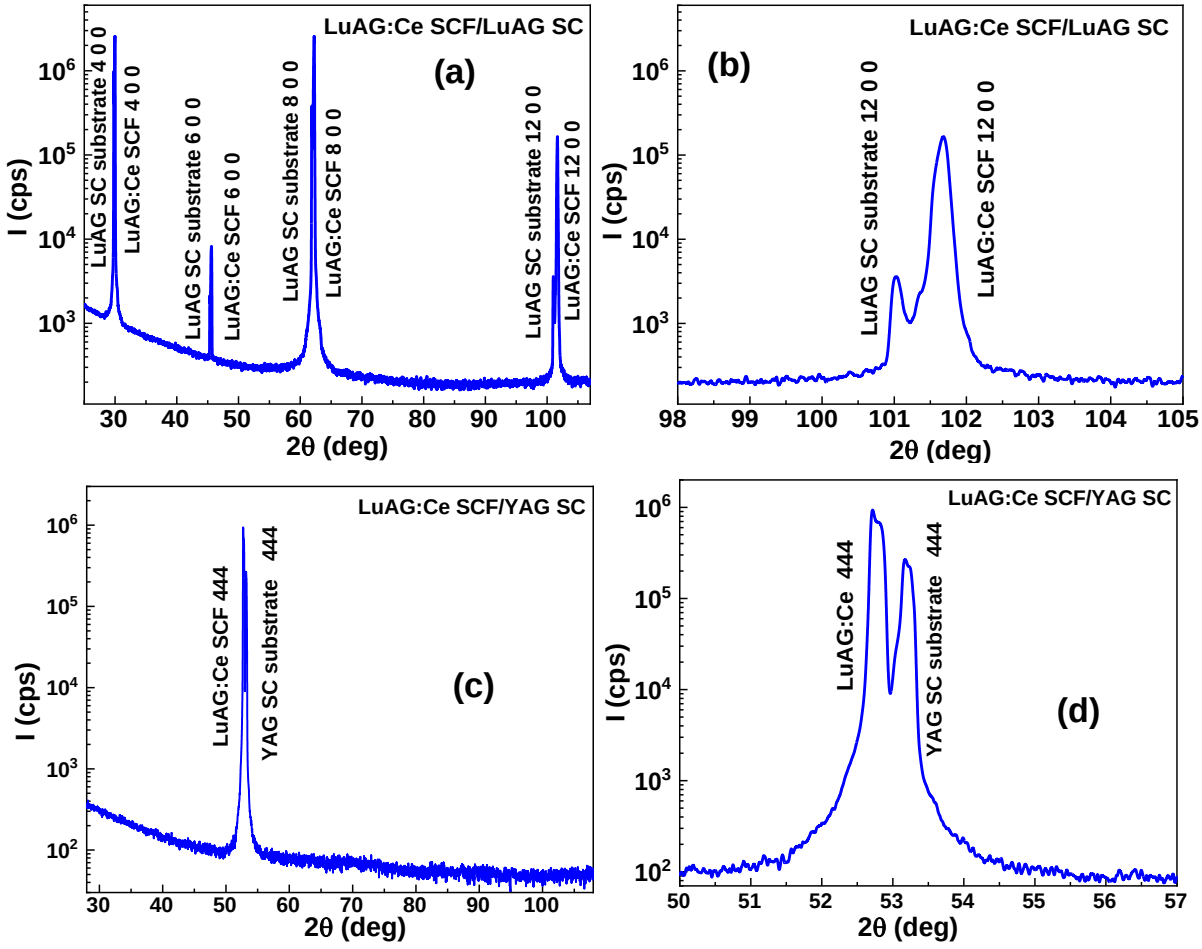

Fig. 2. θ/2θ XRD pattern of (1 0 0) planes of LuAG:Ce SCF/LuAG SC HE structure (a, b) and (111) plane of LuAG:Ce SCF/YAG SC QHE structure (c, d).

The diffraction pattern shows two types of peaks weakly separated from each other, corresponding to reflections from the film and substrate. The peak from the undoped LuAG SC substrate is slightly shifted towards the smaller angle values due to the increased lattice constant compared with the LuAG:Ce SCF (Fig.2 a, b). The deviation lattice constant of the LuAG:Ce films concerning the substrate aligns with some cumulative effect between the incorporation of larger Ce^{3+} ions with an ionic radius (r^{VIII}) of 1.143 Å into the dodecahedral sites of LuAG host in LuAG :Ce SCF and some incorporation of the large Lu^{3+} cations in the Al^{3+} octahedral side of LuAG lattice in the LuAG crystal substrate (so-called Lu_{Al} antisite defects (AD) formation [17]). Such Lu_{Al} AD are absent in the SCF due to the low temperature of their crystallization [24, 25]. The diffractograms in Fig.2a,b and 2c,d displays reflections belonging to the garnet phase, and no other phases have been detected, which confirms the high quality of the LuAG:Ce HE and QHE films.

To explore the relaxation state of the studied epitaxial films, the ω and ω-2θ scans, along with reciprocal space maps, were conducted in the high-resolution XRD mode. Fig.3 illustrates reciprocal space maps measured around the symmetrical 4 0 0 reflection (Fig.3a) and the asymmetrical 10 4 4 reflection (Fig. 3b) for LuAG:Ce SC/LuAG SC HE structure. The scan from the symmetrical reflection allows determining the out-of-plane lattice constant ($a_{\perp}$), while from the asymmetrical reflection *in-plane* lattice constant ($a_{\parallel}$) can be obtained.

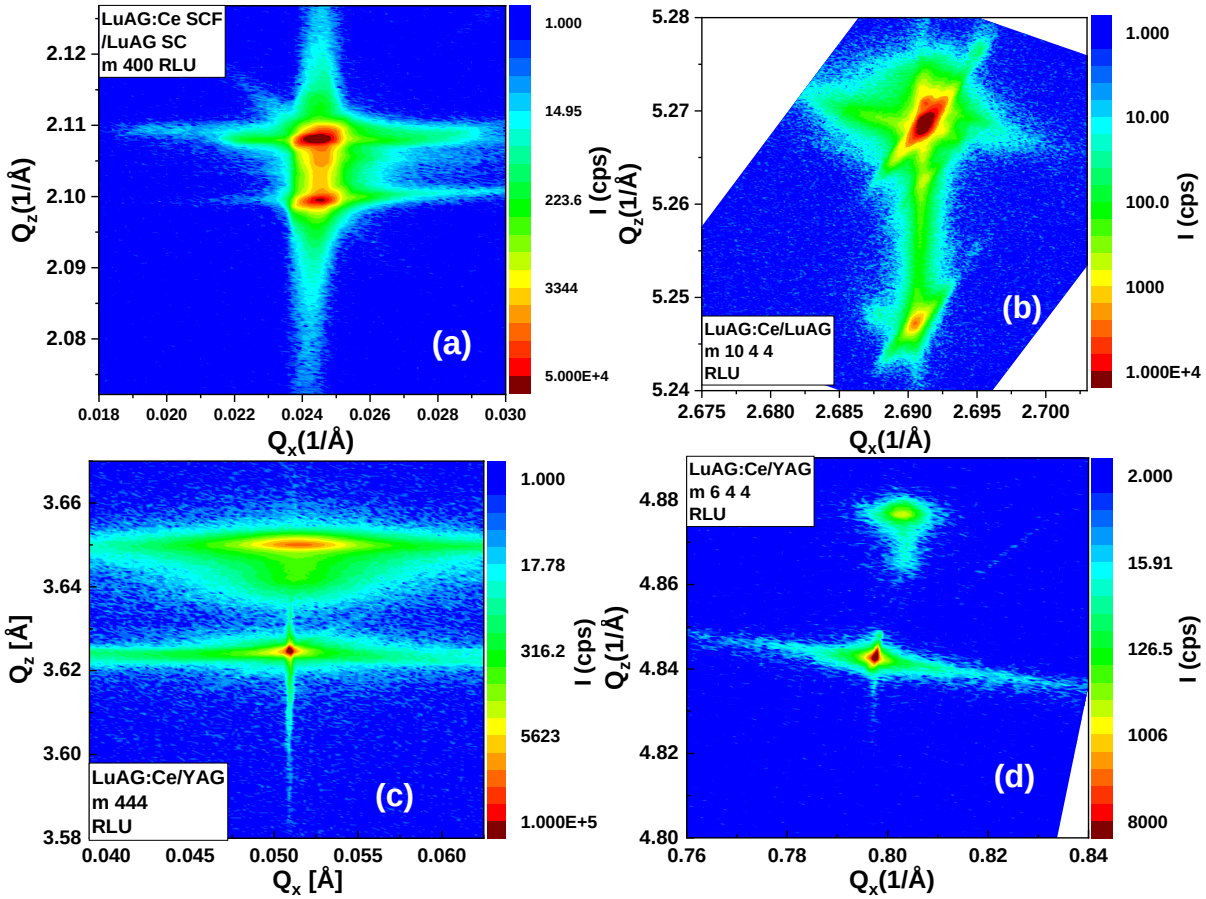

Fig. 3. High-resolution X-ray diffraction (HR-XRD) reciprocal space maps of LuAG:Ce SCF/LuAG SC HE structure (a, b) and LuAG:Ce SCF/YAG SC (c, d) QHE structures. More intense reflection corresponds to the LuAG:Ce SCFs, while a less intense one corresponds to the LuAG and YAG SC substrates accordingly.

The substrate and epitaxial layer lattices and other crystallographic parameters calculated from these results are detailed in Table 1 and Table 2.

Table 1. Results of XRD measurements of LuAG SC substrate, grown by the Czochralski method, and the HE grown LuAG:Ce SCF: a – lattice parameter; d – interplanar distance; FWHM – full width at half of the maximum, m=a_f - a_s/a_s*100% - misfit between lattice constant of SCF $\mathbf{a_f}$ and substrate $\mathbf{a_s}$.

Reflection	**LuAG SC substrate**	**LuAG:Ce SCF**	**misfit m=(a_f - a_s/a_s)*100%**
4 0 0	2θ = 29.8359° $a_{\perp s}$= 11.9685 Å ± 0.0005Å FWHM = 0.0056°	2θ = 29.9619° $a_{\perp f}$=11.9193Å ± 0.0005Å FWHM = 0.0059°	- 0.41 %
10 4 4	2θ = 92.5916° $a_{\parallel f}$=12.2415 Å ± 0.0005 Å	2θ = 92.9866° $a_{\parallel s}$=12.2014Å ± 0.0005Å	- 0.33 %
$\Delta a = a_{\parallel}$-$a_{\perp}$	0.273 Å	0.2821 Å	

The lattice constants determined from the measurement of symmetrical and asymmetrical reflections differ by $\Delta a_S = a_{\parallel}$-$a_{\perp} = 0.273$ Å for the substrate and Δa_{SCF} = 0.2821 for SCF, which indicate the deformation of the substrate and film lattice. In the plane perpendicular to the sample surface (*out-of-plane* mode), the lattice constants are quite consistent with the table values of the LuAG crystal, while in the plane parallel to the surface of the sample (*in-plane*

mode), the values of the lattice constants are higher than the table values [26]. The film lattice parameter in the *in-plane* and *out-of-plane* modes notably differs from that of the substrate, $a_{\perp s} \neq a_{\perp f}$ and $a_{IIs} \neq a_{IIf}$ what is associated with the strain caused by the slight lattice mismatch between the substrate and the epilayer m= - 0.41 % and – 0.33%, respectively (Table 1). The lattice constant of LuAG crystal is influenced by the presence of antisite defects, where rare earth ions substitute cations in octahedral sites. Despite the significant disparity in ionic radii between Lu^{3+} (0.861 Å) and Al^{3+} (0.535 Å) in a 6-fold coordination environment, these defects can occur at relatively high concentrations (from 0.12 up to 0.6 at.% using different estimation methods of AD concentration) [23, 27]. The substantial difference in the radii means that even a relatively small concentration of rare earth antisite defects can impact the lattice parameter of the garnet crystal. In epitaxial LuAG films, it is assumed that the concentration of Lu_{Al} AD is fully absent due to the low temperature of SCF growth [6, 28]. The full-width half-maxima (FWHMs) of the diffraction peaks in the HE SCF are comparable to those of the substrate crystal, suggesting a high level of perfection of SCF.

For QHE growth mode, specifically for LuAG:Ce SCF grown on YAG substrate, the distinct compositions of the film and substrate lead to an anticipated mismatch (Fig. 3b). The absence of cracks in the samples suggests that the film is either (i) in a fully relaxed state or (ii) the relaxation mechanism takes place through the generation of dislocations or (iii) occurs gradually in the transition layer between the substrate and the film. In particular, to confirm this, measurements of HR-XRD reciprocal space maps were carried out for QHE structure, where, according to the literature values of the lattice constant of YAG (12.0088 Å) [29] and LuAG (11.90 Å), a misfit (m= (a_{SCF}-a_{sub})/a_{sub}×100) of about 0.83 % is expected [17, 30] (Fig. 3, c and d). Accordingly, paedomorphic growth of the film is not expected, and the different Q_x coordinates in the HR-XRD reciprocal space map around the asymmetrical 664 diffraction peak preindicates a completely relaxed structure [26].

Table 2 provides a comprehensive overview of the lattice and other crystallographic parameters for both the YAG SC substrate and LuAG:Ce QHE SCF, as derived from the obtained results.

Table 2. Result of XRD measurements of YAG SC substrate, grown by the Czochralski method, and the LuAG:Ce SCF, grown in HE mode: *a* – lattice parameter; d – interplanar distance; FWHM – full width at half of the maximum, m=a_f - a_s/a_s*100% - misfit between lattice constant of SCF **a_f** and substrate **a_s.**

Reflection	**YAG SC substrate**	**LuAG:Ce SCF**	**misfit m=(a_f - a_s/a_s)*100%**
444	2θ = 53.1679° $a_\perp$ =11.9254 ± 0.0005, Å FWHM = 0.0059°	2θ = 52.7729° $a_{\perp S}$ = 12.0082± 0.0005, Å FWHM = 0.0802°	+ 0.69 %
644	2θ = 74.6787° $a_\parallel$= 11.9128 ± 0.0005, Å	2θ = 73.8638° $a_{\parallel s}$ =12.0252 ± 0.0005, Å	+ 0.944 %
$\Delta a = a_\parallel - a_\perp$	- 0.0126 Å	+ 0.017 Å	

The lattice constants determined from the measurement of *in-plane* and *out-of-plane* reflexes differ only by Δa_s = - 0.0126 Å for the substrate and Δa_{SCF} = 0.017 Å for SCF, which are significantly smaller than in the case of LPE grown LuAG SCF/LuAG SC structure. The LuAG:Ce QHE SCF lattice parameters corresponding to the measurements *in- plane* and *out-*

plane orientations significantly differ from those of the YAG substrate, which is associated with the strain caused by the lattice mismatch between the substrate and the epilayer m= - 0.69 % and – 0.935 %, respectively (Table 2).

It is worth noting that if the LuAG:Ce SCF/YAG QHE structure is strained, the lateral lattice parameters of the film would be identical to the substrate. However, from the analysis of the *in-plane* lattice constants for the film and substrate, we have found that the lateral lattice constant of the film $a_{\parallel}$ is significantly different from the value for bulk LuAG crystal substrate. Therefore, we can conclude that LuAG:Ce SCF/YAG QHE structure *is fully relaxed* [31]. Meanwhile, in this case, a slight deformation of the cubic lattice is observed, manifesting the inequality of *in-plane* and *out-of-plane* lattice constants of both substrate and film.

In our previous studies, using high-resolution scanning transition electron microscopy [17] it was demonstrated that the transition layer with 5-6 nm thickness occurs onto the SCF/substrate interface. In this transition layer, the transformation from YAG to LuAG crystal lattice can be considered as a $Y_{3-x}Lu_xAl_5O_{12}$ solid solution, where x varies from 0 to 1 [17]. Furthermore, the relaxation of stresses associated with differences in the garnet lattices in the epitaxial structures occurs in the *transition region* with a thickness of tens of micrometers for both sides of the fragile SCF/substrate interface. In each case, such differences in the structural properties between HE and QHE structures can impact the luminescence properties of these materials. Particular interest lies in the study of epitaxial structures at high pressures, as hydrostatic pressure on layered materials with different elastic constants can manifest in diverse trends in their luminescent properties.

2.2. Absorption spectra

The absorption spectra of LuAG:Ce SCF/LuAG SC HE structure and LuAG:Ce SCF/YAG SC QHE structure show significant similarity (Fig. 4). The main absorption bands peaked at 346 nm and in 447.5 and 448.5 nm, respectively, are related to the intrinsic transitions from the $4f(^2F_{5/2})$ level of ground state to $5d_1$ and $5d_2$ (^2E) excited levels of Ce^{3+} ions (E_1 and E_2 bands, respectively) [5, 23] (Fig.4).

Meanwhile, the maximum of E_1 bands corresponding to the $4f\text{-}5d_{1,2}$ transitions is slightly but measurably shifted by 1nm in the long-wavelength range for LuAG:Ce QHE SCF. For this reason, the difference ΔE in the position of E_1 and E_2 absorption bands, proportional to crystal field strength in the dodecahedral position of garnet lattice and is equal to 0.8115 and 0.8176 eV, respectively, is very small (6.1 meV) (Fig.4). Meanwhile, even such small change of ΔE value may be associated with some difference in local perturbations in the crystalline lattice for LuAG :Ce SCF, grown in *QHE mode*, in comparison with LuAG:Ce SCF, grown in *HE procedure*.

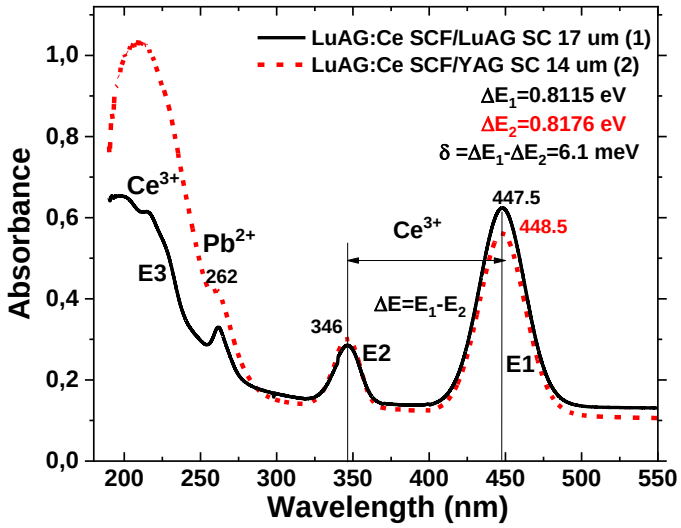

Fig.4. RT absorption spectra of LuAG:Ce SCF/LuAG SC HE structure (1) and LuAG:Ce SCF/YAG SC QHE structure (2).

The bands peaked at 230 nm (E3) corresponding to intrinsic transitions from the 4f($^2F_{5/2}$) level to $5d_1$ and $5d_2$ ($^3T_{2g}$) excited levels of Ce^{3+} ions. The absorption bands peaked at 262 nm and 210 nm corresponding to the $^1S_0 \rightarrow {}^3P_1$ and $^1P_1$ transitions, respectively, of Pb^{2+} flux-related dopants in the LuAG:Ce SCFs under study grown from PbO-based flux.

2.3. Luminescent properties

The photoluminescence (PL) and photoluminescence excitation (PLE) spectra of Ce^{3+} doped LuAG:ce films grown onto LuAG SC and YAG SC substrates exhibit remarkable similarity (Fig. 5). The main excitation bands with the maxima peaked at the 343 nm and in 445.5–447.5 nm range are assigned to the intrinsic transitions from the 4f($^2F_{5/2}$) level of ground state to the $5d_1$ and $5d_2$(^2E) excited levels of Ce^{3+} ions (E_1 and E_2 bands, respectively) [5, 17, 23] (Fig. 5). However, the maxima of these bands corresponding to the 4f-$5d_{1,2}$ transitions slightly differs by a few nanometers for the comparable samples. At the same time, there is a distinct difference (2 nm) in the position of both mentioned transitions, being equal to 343/343 nm and 445.5/447.5 nm for the 4f-$5d_1$ (E_2) and 4f-$5d_2$ (E_1) bands in LuAG:Ce HE SCF and LuAG:Ce QHE SCF, respectively. The difference between the positions of the mentioned bands $\Delta E = E_2 - E_1$, equal to 0.83 and 0.842 eV, is proportional to crystal field strength in the decahedral position of the garnet lattice. The change of this value (0.012 eV) in the excitation spectra (Fig. 5) is larger than the respective value obtained from the absorption spectra (Fig. 4). Such differences in the position of E_2 band and ΔE values also may be associated with different local perturbations in the crystalline lattice for LuAG:Ce SCF/YAG SC QHE structure in comparison with LuAG:Ce SCF/LuAG SC HE counterpart.

PL spectra show the double dominant emission bands in the green-yellow range, related to the allowed $5d^1 \rightarrow 4f(^2F_{5/2;7/2})$ transitions of Ce^{3+} ion in the LuAG host. For LuAG:Ce HE SCF and LuAG:Ce QHE SCF, there is a slight deviation in the shape of these two bands and their maxima. Namely, the position of the low-energy Ce^{3+} emission band at 502.5 nm for the QHE structure is redshifted at 2.5 nm with respect to the corresponding peak for the HE structure, while the positions of the high-energy bands remain the same. Furthermore, the center of Ce^{3+} emission band at FWHM is also notably redshifted from 544.5 to 546 nm (0.006 eV) for LuAG:Ce QHE

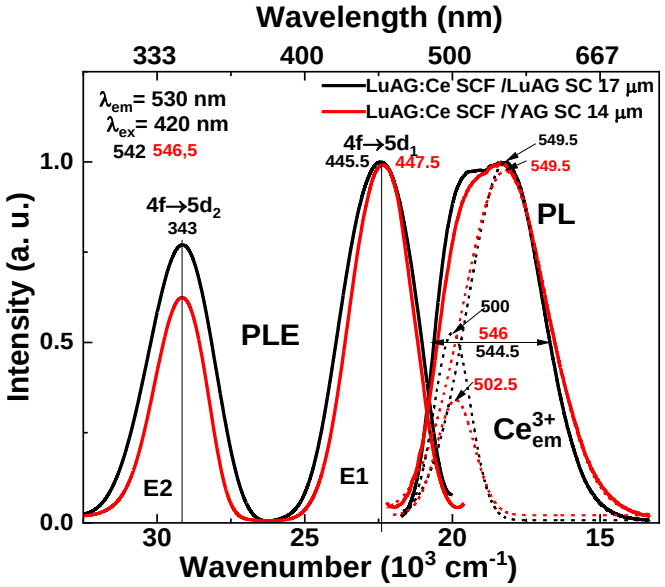

Fig. 5. PL and PLE spectra of LuAG:Ce SCF, LPE grown onto LuAG (black) and YAG (red) SC substrates, respectively. Ce^{3+} luminescence bands are deconvoluted onto two sub-bands (dashed curves) related to the $5d^1 \rightarrow 4f(^2F_{5/2;7/2})$ transitions.

SCF concerning LuAG:Ce HE SCF counterpart (Fig. 5). That corresponds to larger crystal field in the case of LuAG:Ce QHE SCF and coherent with quite large $\Delta E = E_2 - E_1$ value obtained from respective absorption and PLE spectra of this SCF sample.

Fig. 6 a and b show temperature-dependent PL spectra upon excitation at 440 nm of LuAG:Ce SCFs, LPE grown on LuAG and YAG substrates, respectively. At low temperatures in LuAG:Ce, the emission transitions associated with Ce^{3+} ions are distinctly separated and visible, contributing to well-defined spectral features. As the temperature increases, the spectra inhomogeneously broaden, and the two emission bands are not further resolved. Fig. 6c shows the temperature-dependent emission intensity integrated into whole spectra ranges. For both samples, the total intensity consistently decreases with temperature, except in the 200-300 K region, where the PL intensity increases, most likely due to thermal electron de-trapping caused by the defect centers. This deviation is more prominent for LuAG:Ce QHE SCFs.

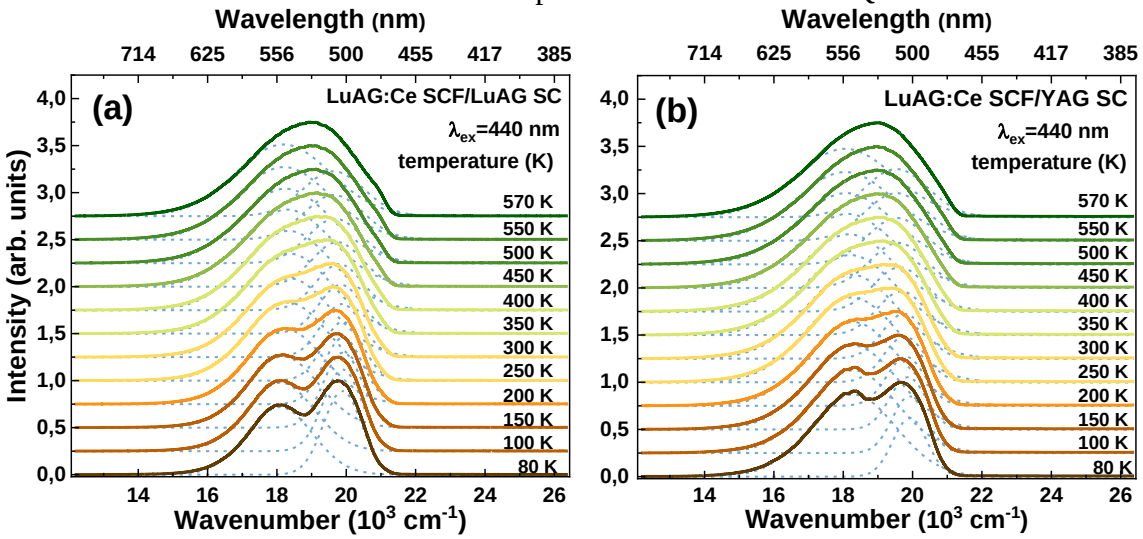

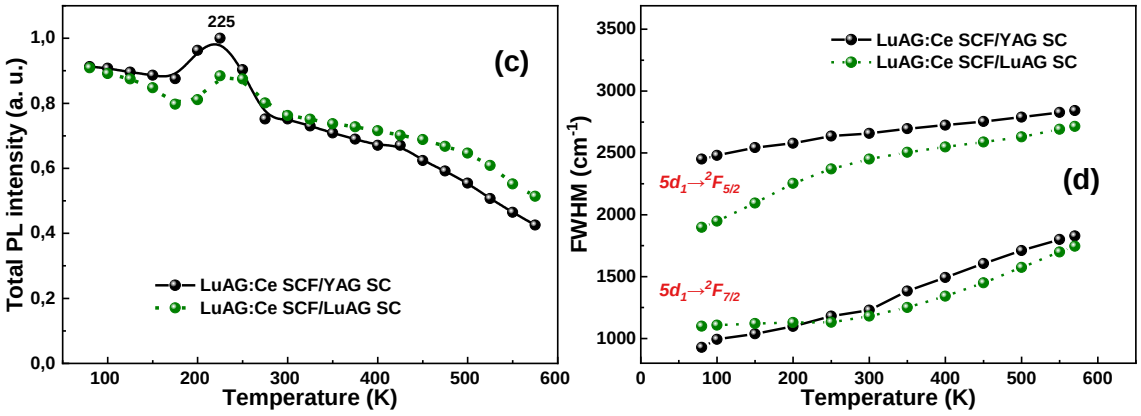

Fig. 6. Temperature-dependent luminescence spectra of Ce^{3+} in LuAG:Ce SCF/LuAG SC HE structure (a) and LuAG:Ce SCF/YAG SC QHE structure (b). Temperature dependence of the Ce^{3+} emission intensity (c) and FWHM of Ce^{3+} luminescence peaks associated with the $5d \rightarrow {}^2F_{5/2,7/2}$ transitions (d) in both epitaxial structures.

The decay profiles of the Ce^{3+} luminescence in the 10-300 K temperature range for both samples are presented in Fig.7a and b. The profiles of the LuAG:Ce QHE SCF deviate from linearity in the logarithmic scale; hence, the two-components function (1) was used for fitting the decay curves at different temperatures

$$I(t) = I_0 \exp(-t/\tau 1) + I_0 \exp(-t/\tau 2), \quad (1)$$

where $I(t)$ is the emission intensity at time t, I_0 is the initial intensity, and τ_1 and τ_2 are luminescence decay times.

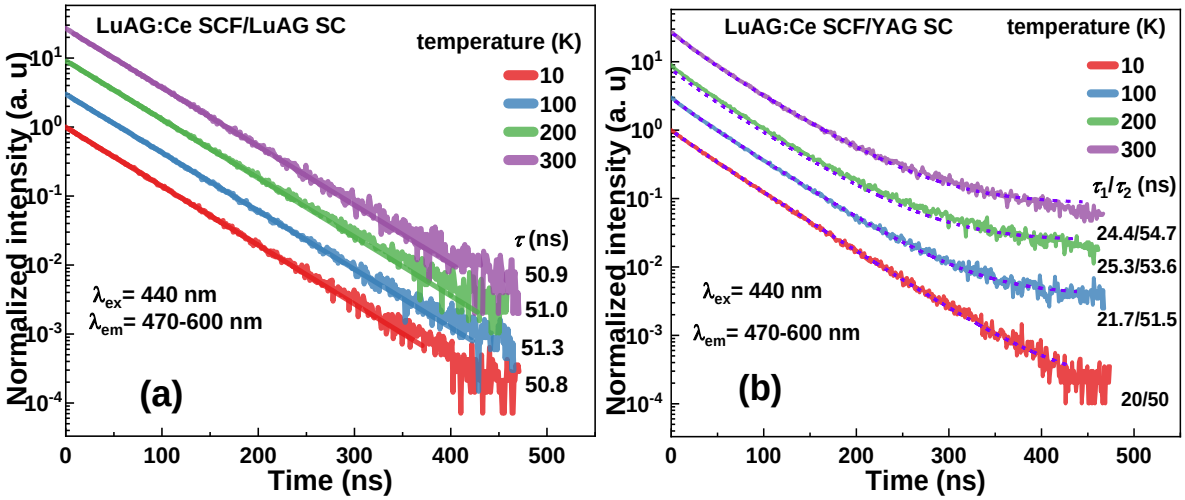

Fig. 7. Decay kinetics of the Ce^{3+} luminescence in LuAG:Ce HE SCF (a) and LuAG:Ce QHE SCF (b) at different temperatures.

The luminescence decay profiles of the LuAG:Ce HE SCF are relatively linear in logarithmic scale (Fig. 7a); hence, function (1) with one decay component was used for fitting. The comparable decay time values τ_1, around 51 ns, clearly demonstrate a weak temperature dependence of the decay curves for this sample.

As shown in Fig. 7b, both decay times of LuAG:Ce QHE SCF show weak temperature dependences and vary between 20-24.4 ns and 50-54.7 ns, respectively. The decay times of the second component are close to the previously reported values of 51 ns for the LuAG:Ce HE SCF (Fig. 7a). The presence of fast decay components in the range of 20-24.4 ns indicates the presence of the energy transfer from Ce^{3+} to some undefined centers in the QHE structure. Taking into

account that the LuAG:Ce QHE SCF is characterized by a higher content of Pb^{2+} flux-related impurity (Fig. 4, curve 2), it is most likely that these unknown centers are Ce^{4+}-Pb^{2+} pairs with local charge and volume compensation [32]. As shown in several recent works [33, 34], the decay kinetics of cerium luminescence under excitation of such pair centers is much faster than in the case of luminescence of undisturbed Ce^{3+} ions. The temperature dependences of τ_1 and τ_2 values (Fig. 7b) may also indicate the formation of Ce^{4+}-Pb^{2+} pairs, which have lower temperature stability than in the case of Ce^{3+} centers.

RT PL spectra of Ce^{3+} in the LuAG:Ce HE SCF and LuAG:Ce QHE SCF under excitation at 442 nm in the pressure range from ambient to 19 GPa are presented in Fig. 8a and 8b, respectively. The elevation in pressure is associated with a notable redshift in the luminescence spectra. Also, with the increase in pressure, the contribution of the $5d\rightarrow{}^2F_{7/2}$ transition increases compared to the $5d\rightarrow{}^2F_{5/2}$ transition. A similar effect was observed previously in Ce^{3+} doped in YAG [35], GSAG [36] and AlN [37].

The redshift observed in the Ce^{3+} luminescence during high-pressure experiments is linked to the compression and potential distortion of the crystal lattice. This spectral shift can be attributed to the *three primary physical mechanisms*: (i) a downward shift of the barycenter (centroid) of 5d levels, ε_c, in comparison to the free ion, (ii) an increase in the crystal field splitting of the 5d states, ε_{cfs}, and (iii) distortion of the oxygen polyhedron surrounding Ce^{3+} from its cubic symmetry.

To conduct a comprehensive examination, the PL spectra were subjected to a decomposition process into two Gaussian bands attributed to the transition from the excited state from $5d_1$ to the ground electronic configuration ($4f_1$) states of Ce^{3+}, specifically the ${}^2F_{7/2}$ and ${}^2F_{5/2}$ states. The determined energy gap between the subbands remains nearly constant and is approximately 2000 cm^{-1}, consistent with the energy separation between these levels, suggesting a lack of increasing distortion of the Ce^{3+} local environment. The peak positions as a function of pressure are shown in Fig. 8c. The filled outer shells afford significant shielding to the 4f electrons, suggesting minimal changes in their energy level positions under pressure. In contrast, the 5d electrons are considerably influenced by the crystal field. Consequently, variations in pressure predominantly impact the luminescence peak energies by reflecting alterations in the position of the 5d energy levels from which the emission originates.

As shown in Fig.8c, the HE and QHE grown LuAG:Ce SCFs demonstrated different trends of the dependence of the Ce^{3+} luminescence band positions on the high-pressure value. Namely, practically linear dependence for the wavenumber of Ce^{3+} emission band on pressure was observed LuAG:Ce QHE SCF in the wide (0-20 GPa) range with -148±3 cm^{-1}/GPa slope (Fig.7c). On the contrary, similar dependence for LuAG:Ce SCF/YAG SC homoepitaxial structure possess at least three specific ranges (0- 5 GPa, 7.3-14.5 GPa and >17-19.2 GPa) with different slopes of wavenumber/pressure dependences which are equal to 155±7 cm^{-1}/GPa, 162±9 cm^{-1}/GPa and 296±12 cm^{-1}/GPa, respectively (Fig. 8c).

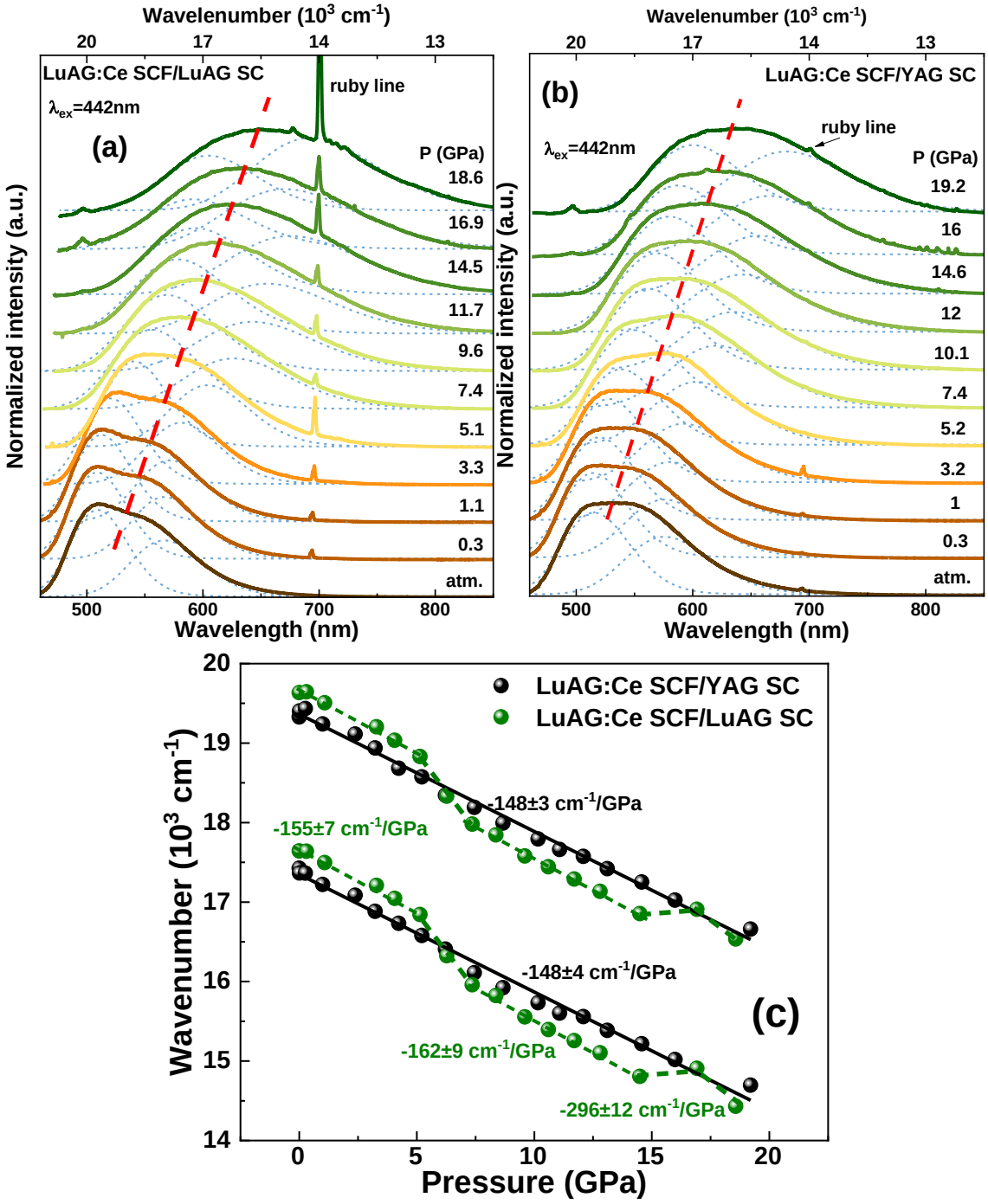

Fig. 8. RT luminescence spectra of Ce^{3+} in LuAG:Ce HE SCF (a) and LuAG:Ce QHE SCF (b) structures under high pressure. (c) - energies of Ce^{3+} luminescence peaks associated with the $5d \rightarrow {}^2F_{5/2,7/2}$ transitions versus pressure in both epitaxial structures under study.

Fig. 9 shows the decay time of the Ce^{3+} luminescence in LuAG:Ce HE SCF (a) and LuAG:Ce QHE SCF (b) obtained for different pressures at RT. It was observed that irrespective of the applied pressures, the luminescence decays consistently followed a single exponential pattern. Observations indicate that the Ce^{3+} luminescence decay within the LuAG host exhibits a subtle sensitivity to pressure, as illustrated in Fig. 9. It is evident that the decay time non-monotonically increases with higher pressure. Namely, two ranges of decay time changes are observed for LuAG:Ce HE SCF: from ambient pressure to 6 GPa and 6 to18 GPa with notably different slopes in both ranges being equal to 0.051 ns/GPa and 0.151 ns/GPa, respectively (Fig. 9c). The changes of the decay time are significantly complicated for LuAG:Ce QHE SCF

in comparison with their HE counterpart. Indeed, even three ranges of decay time changes are observed for QHE structure: from ambient pressure to 6 GPa, from 6 to 13 GPa, and from 13 to 16 GPa with notably different slopes in these ranges being equal to -0.011 ns/GPa, 0.163 ns/GPa and 0.1 ns/GPa, respectively (Fig. 9c).

The increase of the Ce^{3+} luminescence decay times is related to the decrease of nonradiative decay probability due to the pressure-induced increase of the band-gap of LuAG host [38, 39]. The increase of the band-gap energy increases the energy distance between the Ce^{3+} luminescent 5d states and the bottom of the conduction band, decreasing the probability of autoionization of Ce^{3+} 5d states [40].

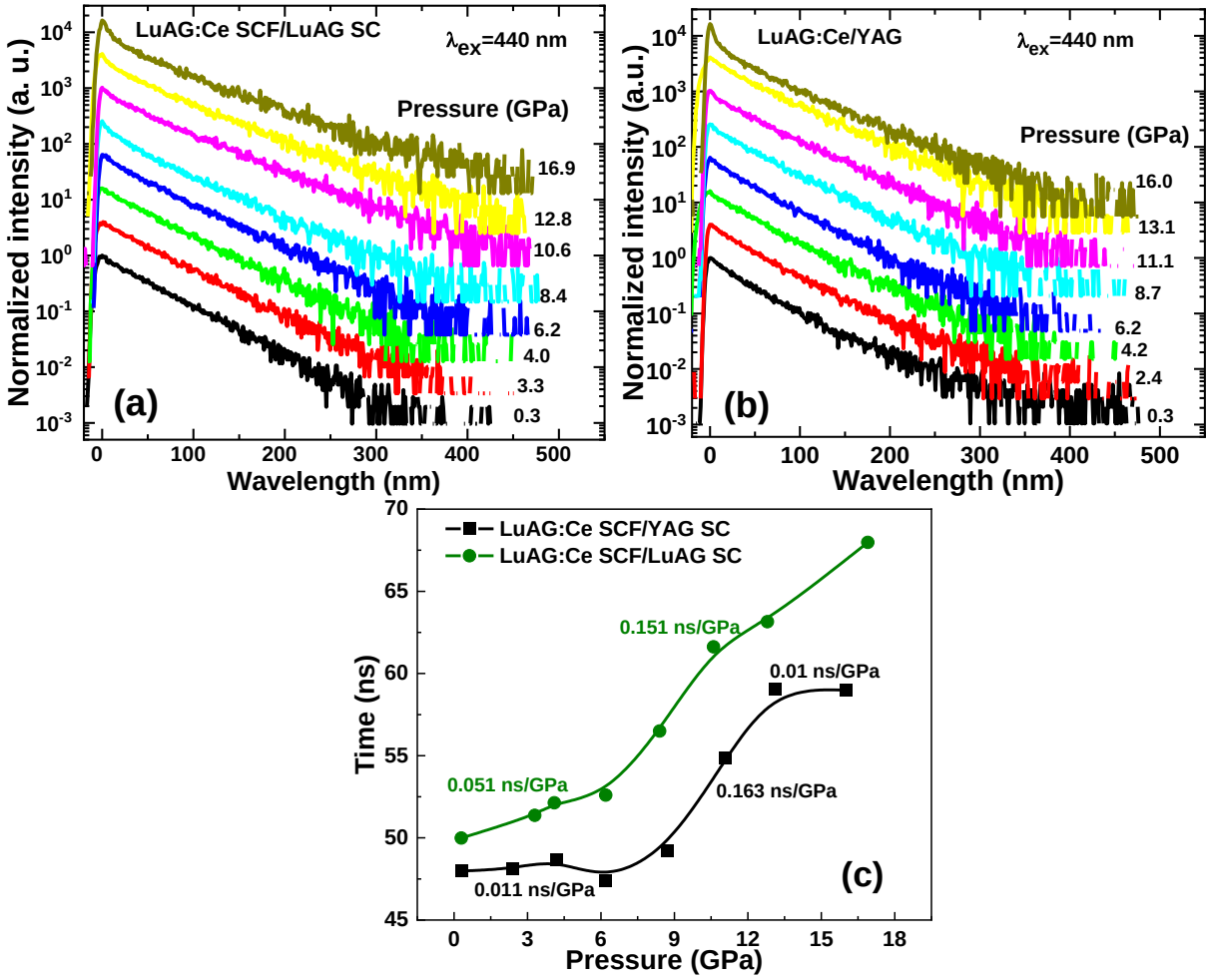

Fig. 9. Pressure dependence of decay profiles (a, b) and decay time (c) of the Ce^{3+} luminescence obtained at RT in LuAG:Ce HE SCF (a) and LuAG:Ce QHE SCF (b).

2.4. Photoconductivity properties

Fig.10, curve 1 shows the photoconductivity excitation (PCE) spectra of LuAG:Ce SCF/ LuAG SC HE epitaxial structure in comparison with reference LPE grown GGG:Ce SCF/GGG HE counterpart [41]. Apart from a slight elevation at around 300, 346 and 426 nm, no noticeable photocurrent was detected in the RT range. Furthermore, LuAG:Ce SCF/YAG SC QHE epitaxial structure does not show any measurable photocurrent (Fig.10, curve 2). In opposite, the reference GGG:Ce SCF shows an distingueshed structure of the PCE spectra (Fig.10, curve 3) with two bands peaked at 418 nm and 338 nm, most likely related to the 4f-5d transition of Ce^{3+} ions in the GGG, and well-resolved bands peaked at 267 and 300 nm, which probably corresponds to the 4f-

4f transitions of Gd^{3+} cations. The significant difference in the intensity of the PCE spectra of both LuAG:Ce SCFs and GGG:Ce SCF counterpart is most likely due to significant differences in the band gap values of the respective garnet hosts, which are 8.0 and 6.4 eV, respectively [42], as well as the distance between the 5d levels of the Ce^{3+} ions and the bottom of the conduction bands [41, 42]. This means that the ionization of the electron from the excited 5d state of Ce^{3+} ions to the conduction band in GAGG host is much easy than in the case of LuAG garnet.

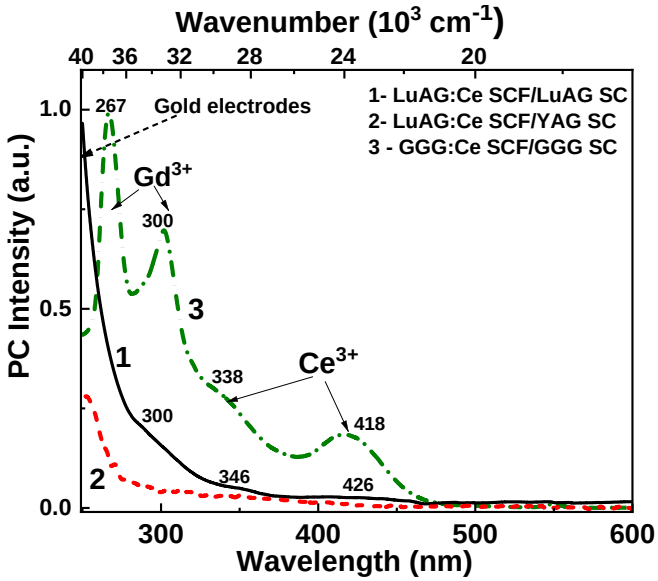

Fig. 10. RT PCE spectra (in log scale) of LuAG:Ce SCF/LuAG SC HE structure (1) and LuAG:Ce SCF/LuAG SC QHE structure (2) in comparison with GAGG:Ce/GGG SC counterpart.

Conclusions

The investigation of the structural and luminescence characteristics of LuAG:Ce single crystalline films grown using the LPE method onto both LuAG and YAG single crystal substrates was performed in this work. The main goals of the research were to study the impact of *homo-epitaxial (HE)* and *quasi-homoepitaxial (QHE)* growth modes on the peculiarities of the luminescence properties of Ce^{3+} ions in LuAG films under ambient and high-pressure conditions.

To explore the relaxation state of the HE and QHE grown LuAG:Ce/LuAG and LuAG:Ce/YAG structures, both ω and ω-2θ XRD scans, and reciprocal space maps were performed in parallel *(in-plane)* and perpendicular *(out-of-plane)* directions concerning film surface. Based on the results of XRD measurements, we conclude that both epitaxial structures *are fully relaxed*. However, even in this case, a slight deformation of the garnet lattices is observed, manifesting the inequality of the *in-plane* (**in**) and *out-of-plane* (**out**) lattice constants of substrates and films. Namely, for LuAG:Ce HE film, lattice constants in the *in-plane* and *out-of-plane* modes differ from those for the LuAG substrate due to the large concentration of Lu_{Al} antisite defects in the LuAG crystal. That is also associated with the strain caused by the film/substrate lattice mismatch $\mathbf{m_{in}}$= –0.41 % and $\mathbf{m_{out}}$= – 0.33%, respectively. The LuAG:Ce QHE film lattice constants *in-plane* and *out-of-plane* significantly differ from those for the YAG substrate, which is associated with the large strain caused by the lattice film/substrate misfit $\mathbf{m_{in}}$= – 0.69 % and $\mathbf{m_{out}}$= – 0.935 %, respectively.

The presence of differences ΔE=6-12 meV in the positions of E_1 and E_2 Ce^{3+} absorption/excitation bands, proportional to crystal field strength in the dodecahedral site of garnet lattice, was observed for LuAG:Ce HE and QHE films, respectively. The center of the Ce^{3+} emission band on FWHM level is red shifted on 6 meV for LuAG:Ce QHE film in comparison with LuAG:Ce HE

counterpart. Such a changes in the positions the Ce^{3+} absorption and emission bands are caused by the differences in local perturbations of garnet hosts in structures, grown in HE and QHE modes.

The Ce^{3+} emission intensity in LuAG:Ce HE and QHE films consistently decreases with temperature in the 10-300 K range. The decay time of the Ce^{3+} luminescence in LuAG:Ce HE film demonstrates a weak temperature dependence in this range. However, the Ce^{3+} decay kinetic in LuAG:Ce QHE film show a notable deviation from the linearity and weak temperature dependences of the decay time presumable due to formation of Ce^{3+}-Pb^{2+} pair centers.

The non-monotonical redshift of the Ce^{3+} emission band and the decrease of the Ce^{3+} decay time are observed in both LuAG:Ce HE and QHE films, under increasing the pressure from ambient to 19 GPa due to the compression and distortion of the crystal lattice. The red shift changes of the Ce^{3+} emission band on pressure are more complicated for LuAG:Ce HE film and contain three ranges with different slopes (-155, -162 and -296 cm^{-1}/GPa), in comparison with QHE counterpart with a linear slope -148cm^{-1}/GPa. In turn, two ranges of Ce^{3+} decay time changes are observed for LuAG:Ce HE film with different slopes of 0.051 and 0.151 ns/ GPa in comparison QHE film where three ranges of decay time changes are found with various slopes of 0.011, 0.163 and 0.1 ns/GPa.

Photocurrent excitation spectra of LuAG:Ce HE and QHE films show very weak intensity in comparison with reference GGG:Ce film due to large LuAG band gap than that in GAGG garnet.

The above-mentioned variations in structural, luminescent, and photocurrent characteristics of LuAG:Ce films at various temperatures and pressures are caused by the differences in local perturbations in the crystalline lattice for both structures, grown in HE and QHE modes onto LuAG and YAG substrates, respectively.

Funding

The work was performed in the frame of Polish NCN 2019/33/B/ST3/00406 and 2022/45/B/ST8/01757 projects and partly in the frame of NCN 2022/47/I/ST8/02600 and Regional Excellence Initiative RID/SP/0048/ 2024/01 projects.

Author Contributions

Anton Markovskyi, Yurii Syrotych, Natalia Majewska and Mikołaj Kamiński conducted measurements of SCFs, analyzed experimental materials, and drafted the manuscript. Vitalii Gorbenko performed the growth of SCFs using the LPE method. The XRD measurements were performed by Alexandra Wierzbicka. Andrzej Suchocki and Sebastian Mahlik analyzed the results of the paper and edited the final version of the manuscript. Yuriy Zorenko performed the conception of the work, corrected the text manuscript, and wrote conclusions.

Conflict of Interest

The authors declare no conflict of interest.

References

[1] M. Nikl, A. Yoshikawa, K. Kamada, K. Nejezchleb, C.R. Stanek, J.A. Mares, K. Blazek, Development of LuAG-based scintillator crystals – A review, Progress in Crystal Growth and Characterization of Materials 59 (2013) 47–72. https://doi.org/10.1016/j.pcrysgrow.2013.02.001.

[2] V. Khanin, A. Meijerink, A.J. Houtepen, H.J.B. Jagt, D.K.G. De Boer, Photosaturation in Luminescent LuAG:Ce Garnet Concentrator Rods, Advanced Photonics Research 2 (2021) 2100055. https://doi.org/10.1002/adpr.202100055.

[3] C. Dujardin, C. Mancini, D. Amans, G. Ledoux, D. Abler, E. Auffray, P. Lecoq, D. Perrodin, A. Petrosyan, K.L. Ovanesyan, LuAG:Ce fibers for high energy calorimetry, Journal of Applied Physics 108 (2010) 013510. https://doi.org/10.1063/1.3452358.

[4] P.A. Cutler, Synthesis and Scintillation of Single Crystal and Polycrystalline Rare-Earth-Activated Lutetium Aluminum Garnet, (n.d.).
[5] T. Yanagida, Y. Fujimoto, Y. Yokota, A. Yoshikawa, T. Ishikawa, H. Fujimura, H. Shimizu, H. Yagi, T. Yanagitani, Scintillation properties of LuAG (Ce) ceramic and single crystalline scintillator, in: IEEE Nuclear Science Symposuim & Medical Imaging Conference, IEEE, Knoxville, TN, 2010: pp. 1612–1614. https://doi.org/10.1109/NSSMIC.2010.5874048.
[6] Yu. Zorenko, V. Gorbenko, I. Konstankevych, A. Voloshinovskii, G. Stryganyuk, V. Mikhailin, V. Kolobanov, D. Spassky, Single-crystalline films of Ce-doped YAG and LuAG phosphors: advantages over bulk crystals analogues, Journal of Luminescence 114 (2005) 85–94. https://doi.org/10.1016/j.jlumin.2004.12.002.
[7]J. Cai, D. Zhu, D. Hu, R. Kučerková, A. Beitlerova, Z. Dai, T. Xie, W. Chewpraditkul, M. Nikl, Z. Zhang, J. Li, Characterization of Ce,Ca:LuAG ceramic scintillators fabricated from co-precipitated powders, Optical Materials 133 (2022) 113051. https://doi.org/10.1016/j.optmat.2022.113051.
[8] Q. Wen, Y. Wang, C. Zhao, L. Xu, X. Wang, Y. Xu, S. Lin, X. Liang, J. Liu, W. Xiang, Ultrahigh Power Density LuAG:Ce Green Converters For High-Luminance Laser-Driven Solid State Lighting, Laser&Amp; Photonics Reviews 17 (2023) 2200909. https://doi.org/10.1002/lpor.202200909.
[9] J. M. Robertson and M. W. van Tol, Epitaxially grown monocrystalline garnet cathode ray-tube phosphor screens, Appl. Phys. Letts, 37 (5), 471, 1980; https://doi.org/10.1063/1.91728
[10] J.M. Robertson, M.W. Van Tol, W.H. Smits, J.P.H. Heynen. Colourshift of the Ce^{3+} emission in monocrystalline epitaxially grown garnet layers. Philips . J. Res. 1981. V. 36. P. 15-30.
[11] L.G. Volzhenskaya, Yu.V. Zorenko, N.I. Patszagan, E.V. Doroshko, Yu.G. Dubov. The peculiarities of luminescence properties of epitaxial garnet luminophores. Journal of Applied Spectroscopy, 44 (1986) 303-306.
[12] Ja.A. Valbis, L.G. Volzhenskaja, Yu.G. Dubov, Yu.V. Zorenko, I.V. Nazar, N.I. Patszagan. Peculiarities of the luminescent properties of single crystallile compounds of $Y_3Al_5O_{12}$, growm from the melt and melt-solution. Optics and Spectroscopy. 63 (1987) 1058-1063.
[13] Yu. Zorenko, V. Gorbenko, I. Konstankevych, B. Grinev, M. Globus. Scintillation properties of $Lu_3Al_5O_{12}$:Ce single crystalline films. Nuclear Instruments & Methods in Physics Research A. A486 (2002) 309-314. https://doi.org/10.1016/S0168-9002(02)00725-8
[14] Yu. V. Zorenko, I. V. Konstankevich, V. I. Gorbenko and P. I. Yurchishin. Preparation, Luminescence Properties, and Application of Scintillators Based on $Lu_3Al_5O_{12}$:Ce Single Crystal Films. Journal of Applied Spectroscopy. 69 (2002) 769-776; https://doi.org/10.1023/A:1021521416098.
[15] M. Kučera, K. Nitsch, M. Nikl, M. Hanuš, S. Daniš, Growth and characterization of YAG and LuAG epitaxial films for scintillation applications, Journal of Crystal Growth 312 (2010) 1538–1545. https://doi.org/10.1016/j.jcrysgro.2010.01.023.
[16] D. Kundaliya, M. Raukas, A.M. Scotch, D. Hamby, K. Mishra, M. Stough, Wavelength converter for an LED and LED containing same, US8937332B2, 2015. https://patents.google.com/patent/US8937332B2/en?oq=8937332%2c+2015 (accessed March 11, 2024).
[17] A. Markovskyi, V. Gorbenko, T. Yokosawa, J. Will, E. Spiecker, M. Batentschuk, J. Elia, A. Fedorov, M. Pakuła, M. Kaczmarek, Y. Zorenko, Structural, luminescence and photoconversion properties of $Lu_3Al_5O_{12}$:Ce single crystalline film phosphors for WLED application, Journal of Alloys and Compounds 929 (2022) 167159. https://doi.org/10.1016/j.jallcom.2022.167159.

[18] C.R. Stanek, K.J. McClellan, M.R. Levy, R.W. Grimes, Extrinsic defect structure of $RE_3Al_5O_{12}$ garnets, Physica Status Solidi (b) 243 (2006). https://doi.org/10.1002/pssb.200642355.
[19] M. Nikl, E. Mihokova, J. Pejchal, A. Vedda, Yu. Zorenko, K. Nejezchleb, The antisite Lu_{Al} defect-related trap in $Lu_3Al_5O_{12}$:Ce single crystal, Physica Status Solidi (b) 242 (2005). https://doi.org/10.1002/pssb.200541225.
[20] Yu. Zorenko, A. Voloshinovskii, V. Savchyn, T. Voznyak, M. Nikl, K. Nejezchleb, V. Mikhailin, V. Kolobanov, D. Spassky, Exciton and antisite defect-related luminescence in $Lu_3Al_5O_{12}$ and $Y_3Al_5O_{12}$ garnets, Physica Status Solidi (b) 244 (2007) 2180–2189. https://doi.org/10.1002/pssb.200642431.
[21] L. Merrill, W.A. Bassett, Miniature diamond anvil pressure cell for single crystal x-ray diffraction studies, Review of Scientific Instruments 45 (1974) 290–294. https://doi.org/10.1063/1.1686607.
[22] S. Mahlik, High-Pressure Study of Phosphors Emission, in: Phosphor Handbook, 3rd ed., CRC Press, 2022.
[23] H. Przybylińska, A. Wittlin, C.-G. Ma, M.G. Brik, A. Kamińska, P. Sybilski, Yu. Zorenko, M. Nikl, V. Gorbenko, A. Fedorov, M. Kučera, A. Suchocki, Rare-earth antisites in lutetium aluminum garnets: Influence on lattice parameter and Ce^{3+} multicenter structure, Optical Materials 36 (2014) 1515–1519. https://doi.org/10.1016/j.optmat.2014.04.015.
[24] V.V. Laguta, A.M. Slipenyuk, M.D. Glinchuk, I.P. Bykov, Y. Zorenko, M. Nikl, J. Rosa, K. Nejezchleb, Paramagnetic impurity defects in LuAG:Ce thick film scintillators, Radiation Measurements 42 (2007) 835–838. https://doi.org/10.1016/j.radmeas.2007.02.033
[25] Yu. Zorenko, E. Zych, A. Voloshinovskii, Intrinsic and Ce^{3+}-related luminescence of YAG and YAG:Ce single crystals, single crystalline films and nanopowders, Optical Materials 31 (2009) 1845–1848. https://doi.org/10.1016/j.optmat.2008.11.026.
[26] F. Euler, J.A. Bruce, Oxygen coordinates of compounds with garnet structure, Acta Cryst 19 (1965) 971–978. https://doi.org/10.1107/S0365110X65004747.
[27] M.Kh. Ashurov, Yu. Voronko, V.V. Osiko, A.A. Sobol, M.I. Timoshechkin, Spectroscopic study of stoichiometry deviation in crystals with garnet structure, Physica Status Solidi (a) 42 (1977) 101–110. https://doi.org/10.1002/pssa.2210420108.
[28] M. Nikl, A. Vedda, M. Fasoli, I. Fontana, V.V. Laguta, E. Mihokova, J. Pejchal, J. Rosa, K. Nejezchleb, Shallow traps and radiative recombination processes in $Lu_3Al_5O_{12}$:Ce single crystal scintillator, Phys. Rev. B 76 (2007) 195121 https://doi.org/10.1103/PhysRevB.76.195121.
[29] Ya. Zhydachevskyy, I.I. Syvorotka, V. Tsiumra, M. Baran, L. Lipińska, A. Wierzbicka, A. Suchocki, Quantum efficiency of the down-conversion process in Bi^{3+}–Yb^{3+} and Ce^{3+}–Yb^{3+} co-doped garnets, Solar Energy Materials and Solar Cells 185 (2018) 240–251. https://doi.org/10.1016/j.solmat.2018.05.037.
[30] M. Kneiß, D. Splith, H. Von Wenckstern, M. Lorenz, T. Schultz, N. Koch, M. Grundmann, Strain states and relaxation for alpha-$(Al_xGa_{\{1-x\}2}O_3$ thin films on prismatic planes of alpha-Al_2O_3 in the full composition range: Fundamental difference of a- and m-epitaxial planes in the manifestation of shear strain and lattice tilt, Journal of Materials Research 36 (2021) 4816–4831. https://doi.org/10.1557/s43578-021-00375-3.
[31] J.W. Matthews, A.E. Blakeslee, Defects in epitaxial multilayers, Journal of Crystal Growth 27 (1974) 118–125. https://doi.org/10.1016/S0022-0248(74)80055-2.
[32] Svetlana Zazubovich, Aleksei Krasnikov, Yuriy Zorenko, Vitali Gorbenko, Vladimir Babin, Eva Mihokova, and Martin Nikl, Luminescence of Pb- and Bi-Related Centers in Aluminum Garnet, Perovskite, and Orthosilicate Single-Crystalline Films. In monography "Nanocomposite, Ceramic, and Thin Film Scintillators", p. 227-287. Pan Stanford Publishing

Pte. Ltd.. Nov. 11, 2016.
[33] V. Gorbenko, T. Zorenko, S. Witkiewicz-Łukaszek, A. Shakhno, A. Osvet, M. Batentschuk, A. Fedorov, Yu. Zorenko. Crystallization and investigation of the structural and optical properties of Ce^{3+} doped $Y_{3-x}Ca_xAl_{5-y}Si_yO_{12}$ single crystalline film phosphors. Crystals, 2021, 11, 788. https://doi.org/10.3390/cryst11070788.
[34] Vitaliy Gorbenko, Tetiana Zorenko, Anna Shakhno, Paweł Popielarski, Andres Osvet, Miroslaw Batentschuk, Alexander Fedorov, Sebastian Mahlik, Tadeusz Leśniewski, Natalia Majewska, Yuriy Zorenko. Single Crystalline Films of Ce^{3+}-Doped $Y_3Mg_xSi_yAl_{5-x-y}O_{12}$ Garnets: Crystallization, Optical, and Photocurrent Properties, Materials, 2023, *16*(5), 1869.
[35] J. Barzowska, M. Grinberg, T. Tsuboi, High Pressure Spectroscopy of Ce Doped YAG Crystal, Radiation Effects and Defects in Solids 158 (2003) 39–47. https://doi.org/10.1080/21040215021000052917.
[36] M. Grinberg, J. Barzowska, Y. Shen, R.S. Meltzer, K.L. Bray, Pressure dependence of electron-phonon coupling in Ce^{3+} -doped $Gd_3Sc_2Al_3O_{12}$ garnet crystals, Phys. Rev. B 69 (2004) 205101. https://doi.org/10.1103/PhysRevB.69.205101.
[37] M. Kamiński, A. Lazarowska, T. Leśniewski, R.-S. Liu, S. Mahlik, Opposite pressure impact on electron–phonon coupling in Eu^{2+} and Ce^{3+} doped AlN, J. Mater. Chem. C 11 (2023) 16264–16270. https://doi.org/10.1039/D3TC03271J.
[38]. Lev-Ivan Bulyk, Ajeesh Kumar Somakumar, Hanka Przybylińska, P. Ciepielewski, Yu. Zorenko, Ya. Zhydachevskyy, I. Kudryavtseva, V. Gorbenko, A. Lushchik, M. G. Brik, Y. Syrotych, S. Witkiewicz-Łukaszek, A. Fedorov, Andrzej Suchocki, Influence of high pressure on Ce^{3+} luminescence in $LuAlO_3$ and $YAlO_3$ single crystals and single crystalline layers, J. Luminescence 252 (2022) 119276 https://doi.org/10.1016/j.jlumin.2022.119276].
[39] A. Kamińska, A. Duzynska, M. Berkowski, S. Trushkin, A. Suchocki, Pressure induced luminescence of cerium doped gadolinium gallium garnet crystal, Phys. Rev. B 85 (2012) 155111; https://doi.org/10.1103/PhysRevB.85.155111
[40] A. Wittlin, H. Przybylińska, M. Berkowski, A. Kamińska, P. Nowakowski, P. Sybilski, Chong-Geng Ma, M.G. Brik, and A. Suchocki, Ambient and high pressure spectroscopy of Ce^{3+} doped yttrium gallium garnet, Optical Materials Express, 5 (2015), 1868-1880. https://doi.org/10.1364/OME.5.001868.
[41] J. Ueda, S. Tanabe. Review of luminescent properties of Ce^{3+}-doped garnet phosphors: New insight into the effect of crystal and electronic structure. Optical Materials: X, 1 (2019) 100018. https://doi.org/10.1016/j.omx.2019.100018.
42. M. Fasoli, A.Vedda, M. Nikl, C. Jiang, B.P. Uberuaga, D.A. Andersson, K.J. McClellan, C.R. Stanek. Band gap engineering for shallow trap removal in $RE_3Al_5O_{12}$ garnets. Phys. Rev., B 84 (2011) 081102(R). https://doi.org/10.1103/PhysRevB.84.081102.